Nucleic Acids Research, 2022 ***1–17***
https://doi.org/10.1093/nar/gkac077

H3K36 methylation and DNA-binding both promote loc4 recruitment and Isw1b remodeler function

Jian Li[1,†], Lena Bergmann [2,†], Andreia Rafael de Almeida[2], Kimberly M. Webb[3], Madelaine M. Gogol[4], Philipp Voigt [3,5], Yingfang Liu [1,6], Huanhuan Liang[1,7,*] and Michaela M. Smolle [2,8,*]

[1]State Key Laboratory of Biomacromolecules, Institute of Biophysics, Chinese Academy of Sciences, 15 Datun Road, Chaoyang District, Beijing 100101, China, [2]Physiological Chemistry, Biomedical Center, Medical Faculty, Ludwig-Maximilian-University Munich, Grosshaderner Str. 9, 82152 Martinsried-Planegg, Germany, [3]Wellcome Centre for Cell Biology, School of Biological Sciences, University of Edinburgh, Edinburgh EH9 3BF, UK, [4]Stowers Institute for Medical Research, 1000 E 50th Street, Kansas City, MO 64110, USA, [5]Epigenetics Programme, Babraham Institute, Cambridge CB22 3AT, UK, [6]School of Medicine, Sun Yat-Sen University, Guangzhou 510275, China, [7]Pharmaceutical Sciences (Shenzhen), Sun Yat-sen University, Guangzhou 510275, China and [8]BioPhysics Core Facility, Biomedical Center, Medical Faculty, Ludwig-Maximilian-University Munich, Grosshaderner Str. 9, 82152 Martinsried-Planegg, Germany

Received February 21, 2021; Revised January 20, 2022; Editorial Decision January 23, 2022; Accepted February 08, 2022

ABSTRACT

The Isw1b chromatin-remodeling complex is specifically recruited to gene bodies to help retain pre-existing histones during transcription by RNA polymerase II. Recruitment is dependent on H3K36 methylation and the Isw1b subunit Ioc4, which contains an N-terminal PWWP domain. Here, we present the crystal structure of the Ioc4-PWWP domain, including a detailed functional characterization of the domain on its own as well as in the context of full-length Ioc4 and the Isw1b remodeler. The Ioc4-PWWP domain preferentially binds H3K36me3-containing nucleosomes. Its ability to bind DNA is required for nucleosome binding. It is also furthered by the unique insertion motif present in Ioc4-PWWP. The ability to bind H3K36me3 and DNA promotes the interaction of full-length Ioc4 with nucleosomes *in vitro* and they are necessary for its recruitment to gene bodies *in vivo*. Furthermore, a fully functional Ioc4-PWWP domain promotes efficient remodeling by Isw1b and the maintenance of ordered chromatin *in vivo*, thereby preventing the production of non-coding RNAs.

INTRODUCTION

DNA is packaged into chromatin, a highly condensed nucleo-protein complex that serves as a substrate for all nuclear, DNA-based processes, such as transcription, replication or DNA repair. During gene transcription by RNA polymerase II (RNAPII) nucleosomes first have to be removed in front of the enzyme and then restored after RNAPII passage, so as to prevent inappropriate access to the underlying DNA sequences by the transcription machinery (1). Organization of chromatin structure is achieved by the concerted actions of histone modifying enzymes, chromatin remodelers and histone chaperones (2).

Many different post-translational histone modifications have been identified, including lysine acetylation and methylation. PTMs can affect chromatin organization directly, for example by altering the electrostatic surface of histones. Alternatively, they can influence chromatin structure indirectly by providing binding platforms for specific reader modules present in many chromatin-associated factors. Over 20 such reader domains have been identified (3).

Remodeling factors use the energy generated by ATP hydrolysis to affect chromatin organization as a consequence of nucleosome sliding, eviction or assembly (4). ISWI (*I*mitation *S*witch) is one of four families of remodeling enzymes that are conserved from yeast to humans. The Iswi remodeler was initially identified in *Drosophila melanogaster* (5) and possesses two homologs in *Saccharomyces cerevisiae*, Isw1 and Isw2 (6). In turn, Isw1 is the catalytic subunit of two distinct remodeling complexes, Isw1a and Isw1b (7). Previous work has shown that the Isw1b chromatin remodeler is involved in retaining H3K36-methylated histones and thereby maintaining proper chromatin organization over gene bodies (8,9). More recently,

*To whom correspondence should be addressed. Tel. +49 89 218077098; Email: michaela.smolle@bmc.med.lmu.de
Correspondence may also be addressed to Huanhuan Liang. Email: lianghh26@mail.sysu.edu.cn
†The authors wish it to be known that, in their opinion, the first two authors should be regarded as Joint First Authors.

Isw1b was implicated in the upkeep of regular phasing of nucleosomal arrays by resolving closely packed dinucleosomes (10). Isw1b consists of two other subunits apart from Isw1, namely Ioc2 and Ioc4 (7). Recruitment of the Isw1 remodelers to different genomic regions depends on these associated subunits. In case of Isw1b, its localization to coding sequences depends on Ioc4. In its absence pre-existing, H3K36 trimethylated histones are lost from ORFs. Deletion of *ISW1* has the same effect (8).

The only domain annotated within Ioc4 is an N-terminal PWWP domain. PWWP domains are part of the Royal superfamily and were originally identified as DNA-binding domains (11–13). Subsequent studies revealed that most PWWP-containing proteins associate with methylated histones via a conserved aromatic cage (3). Most domains examined display a preference for histone H3 trimethylated at Lys36 (H3K36me3), although some bind to H4K20me (Pdp1, HDGF2) or H3K79me3 (HDGF2) (14,15).

While the importance of full-length Ioc4 for Isw1b recruitment and function has been demonstrated previously, we wanted to characterize in more detail the importance of the Ioc4 PWWP domain ($Ioc4_{PWWP}$) in these processes. Therefore, we solved the crystal structure of $Ioc4_{PWWP}$ and related its structural features to $Ioc4_{PWWP}$ functions, both *in vivo* and *in vitro*. We found that full Isw1b remodeling activity is reached in the presence of a functional Ioc4 PWWP domain. Also, recruitment of the Isw1b remodeler through its Ioc4 subunit *in vivo* depends on interactions between $Ioc4_{PWWP}$ and H3K36 methylation as well as DNA binding. Mutants not able to recognize either methylation and/or to bind to DNA display reduced Isw1b remodeling activities, reduced chromatin association of Ioc4 *in vivo* and increased production of non-coding RNAs. This highlights the importance of native $Ioc4_{PWWP}$ interactions for remodeler recruitment and its function in chromatin organization.

MATERIALS AND METHODS

Yeast strains and media

All yeast strains used in this study are listed in Supplementary Table S1. Wildtype *IOC4* was tagged with a 3xFLAG epitope by targeted homologous integration of a PCR product derived from amplification of plasmid p3xFLAG-HIS3 with gene-specific primers. In order to generate yeast strains bearing different mutations of *IOC4*, mutant *IOC4* constructs were first cloned into plasmid p3xFLAG-HIS3, followed by PCR amplification of these cassettes and transformation into wildtype yeast. To generate TAP-tagged yeast strains, the 3xFLAG tag was replaced by targeted homologous integration of a PCR product derived from amplification of plasmid pBS1539 with construct-specific primers. Single deletion of *CHD1* was done by targeted homologous recombination of PCR fragments containing either the hygromycin (*HphB*) or kanamycin (*KanMX*) resistance marker. All strains generated in this study were confirmed by PCR and/or sequencing. Cells were grown at 30°C in YPD.

Yeast growth assay

Yeast strains were inoculated at an OD_{600} of 0.1 from overnight cultures and grown for ca. 5 h at 30°C in YPD until they were growing exponentially. Equal numbers of cells were harvested by centrifugation, washed with ddH_2O and resuspended at an OD_{600} of 0.5 in ddH_2O. Five 6-fold dilutions were prepared for each strain and spotted onto YPD plates ±1 μM propiconazole. Plates were incubated at 30°C for 3–5 days.

Protein purification

For crystallization the Ioc4-PWWP domain (aa 1–178; $Ioc4_{PWWP}$) was overexpressed as an N-terminal fusion with maltose-binding protein (MBP) in *Escherichia coli* BL21 (DE3) by the addition of 0.25 mM IPTG for 20 h at 16°C. MBP-$Ioc4_{PWWP}$ was purified to homogeneity using a sequence of amylose resin affinity, anion exchange and gel filtration chromatography. The wildtype PWWP and mutant $PWWP_{2KE}$ domains were cloned into a pRSF vector with an N-terminal 6xHis-tag. Both proteins were overexpressed in *E. coli* BL21(DE3) by the addition of 0.25 mM IPTG for 20 h at 16°C. Both proteins were purified using nickel-NTA resin and anion exchange chromatography. Full-length Ioc4 (aa1-475), $Ioc4_{2KE}$ and $Ioc4_{\Delta PWWP}$ (aa 179–475) were cloned into a modified pCoofy vector with an N-terminal 6xHis-MBP tag. Proteins were overexpressed in *E. coli* BL21 RIL by addition of 0.25 mM IPTG for 20 h at 16°C and purified using nickel-NTA resin, Heparin adsorption and gel filtration chromatography. Proteins were dialysed exhaustively against buffer D (50 mM phosphate, pH 8.0, 500 mM NaCl, 10% glycerol, 50 mM Arg, 50 mM Glu), flash-frozen in liquid nitrogen and stored at −80°C.

TAP-tagged wildtype and mutant Isw1b chromatin remodelers were purified from *S. cerevisiae*. Yeast were grown in YPD at 30°C until they reached an OD_{600} of 5–7. Cells were harvested by centrifugation (5000 × *g*, 15 min), washed with cold PBS, resuspended in buffer E (40 mM HEPES−KOH, pH7.5, 350 mM NaCl, 10% glycerol, 0.1% Tween-20, 1 mM PMSF, 2 μg/ml leupeptin, 1 μg/ml Pepstatin A) and lyzed using a freezer mill. Lysates were treated with 1 mg Heparin and 250 U of Benzonase (Merck Millipore) for 15 min at room temperature before removing cell debris by centrifugation (31 000 × *g*, 20 min) and ultracentrifugation (208 000 × *g*, 1.5 h). The supernatant was incubated with IgG sepharose (GE Healthcare) at 4°C for 3 h. The resin was washed with buffer E for three times 5 min, resuspended with cleavage buffer (10 mM Tris pH 8.0, 10% Glycerol, 150 mM NaCl, 0.1% IGEPAL CA630, 0.5 mM EDTA, 1 mM DTT) and incubated with TEV protease for 16 h at 4°C. Cleaved protein was diluted with buffer B (10 mM Tris, pH 8.0, 150 mM KCl, 1 mM Magnesium acetate, 1 mM imidazole, 2 mM CaCl2, 10% glycerol, 0.1% IGEPAL CA630, 1 mM DTT) and incubated with calmodulin sepharose (GE Healthcare) for 3 h at 4°C, followed by three 10 min washes with buffer B. Complexes were eluted with buffer EB (10 mM Tris, pH 8.0, 150 mM KCl, 1 mM magnesium acetate, 1 mM imidazole, 10 mM EGTA, 10% glycerol, 0.1% IGEPAL CA630, 0.5 mM DTT), concentrated, flash frozen in liquid nitrogen and stored at −80°C.

Recombinant *Xenopus laevis* histones were expressed, purified and assembled into core histone octamers as described (16). To generate histone H3 containing either unmethylated or trimethylated K36, tail peptides (aa1−44) containing either K36me0 or K36me3 were ligated onto histone $H3_{T45C}$ and used for subsequent core histone octamer assembly (17). For sliding assays methyl-lysine analogue (MLA) $H3_{K36C}$ nucleosomes chemically modified to resemble trimethylated H3K36 were used instead, as described previously (8).

Crystallization and structure determination

Purified MBP-$Ioc4_{PWWP}$ was concentrated to ∼10 mg/ml and used for crystal screening by sitting-drop vapor diffusion at 16°C. Needle-shaped crystals grew in reservoir solution containing 0.1 M potassium thiocyanate, 30% mPEG 2000. Data were collected on beamline BL17U (SSRF, China, $\lambda = 0.979$ Å) and processed using the HKL2000 program suite. Structure of the fusion protein was solved by molecular replace method with the program PHASER, using the MBP structure as a search template. An initial model was automatically built by Phenix Autosol, manually modified with Coot and refined with Phenix Refine. The final model contains two missing fragments, F19 and S43-K91 and has an R_{work} of 17.3% and an R_{free} of 22.9%. Data scaling, refinement, and validation statistics are shown in Supplementary Table S1.

Reconstitution of mononucleosomes, electromobility shift (EMSA) and remodeling assays

DNA fragments measuring either 147 or 215 bp and containing the 601 positioning sequence were PCR amplified from pGEM-3Z/601 (18) using Cy5-labeled primers (Supplementary Table S3). Mononucleosomes were reconstituted from DNA and recombinant core histone octamers by serial dilution as described (16). EMSA assays with reconstituted, K36me0- or K36me3-containing mononucleosomes were performed as described (8,16) using 15 fmol of reconstituted nucleosomes per reaction with increasing concentrations of wildtype and mutant PWWP domains (0–800 nM) or full-length Ioc4 (0–35 nM). Unmodified wildtype nucleosomes (30 fmol) were incubated with increasing concentrations (0–4 μM) of wildtype or mutant PWWP. For DNA EMSAs double-stranded (ds), Cy5-labeled DNA with a length of 30 bp was prepared by heating and annealing complimentary, single-stranded (ss) DNA (Supplementary Table S3). Complexes were separated on 5.0% native PAGE gels (37.5:1) run in 0.4× TBE, 2% glycerol. Gels were scanned using a Typhoon FLA9500 and quantitated with ImageQuant TL (GE Healthcare). Mononucleosome or DNA bands were quantitated for each lane. All lanes containing PWWP or Ioc4 were normalized against input lanes containing mononucleosomes or DNA only. The percentage of nucleosomes or DNA bound was expressed as 100 – % mononucleosomes or DNA for each lane. For nucleosome sliding assays, 10 μl reactions containing 30 fmol mononucleosomes and 10 fmol remodeler were set up in buffer R (50 mM Tris–HCl, pH8.0, 50 mM KCl, 10 mM $MgCl_2$, 1 mM ATP, 0.1 μg/μl BSA, 5mM DTT, 0.5 mM PMSF). Reactions were incubated at room temperature, aliquots removed at various time points and stopped by adding 720 ng plasmid DNA, 500 mM KCl. Nucleosomes were resolved on 7% native PAGE gels (37.5:1) in 0.4× TBE, 2% glycerol. Gels were scanned using a Typhoon FLA9500 and quantitated with ImageQuant TL. Bands representing remodeled mononucleosomes were normalized to their respective input lanes.

Antibodies

The following antibody was used in this study: αFlag M2 (Sigma #F1804).

Chromatin immunoprecipitation, ChIP-qPCR and ChIP-chip microarray analyses

For ChIPs of FLAG-tagged Ioc4 yeast strains were grown in 200 ml of YPD at 30°C, crosslinked and processed for ChIP as described earlier (8). FLAG-tagged Ioc4 was immunoprecipitated as described before (8). Three biological repeats were done for all experiments. Immunoprecipitated DNA was quantitated by qPCR using PowerTrack SYBR Green Master Mix (Thermo Fisher Scientific) and a QuantStudio 5 Real-Time PCR System (Applied Biosystems). Primers are listed in Supplementary Table S3. The mean signal was calculated for each experiment and normalized against input samples at each primer position as internal controls. Input-normalized values were further corrected for variation by normalizing against the mean signals for two control regions (*STE3,* subtelomeric region on chromosome V (*ChrV*)). ChIP-chip assays for the genome-wide distribution of FLAG-tagged Ioc4 were performed as described previously (8), using 8 × 60K yeast genome DNA arrays (Agilent, Array #031697). Arrays were scanned (Agilent DNA Microarray Scanner Model G2505B) and extracted using Feature Extraction software (Agilent) and normalized using median normalization in R software. The normalized data were analysed using a modified gene average analysis (8). ORFs were subdivided into 14 equal sized bins each. Intergenic regions (480 bp up- and downstream of genes) were allocated into three bins each. Microarray enrichment ratios [$\log_2$(IP/input)] for each probe were assigned to the closest bin. For whole-genome average gene plots all probes within a bin were averaged and plotted as mean ± standard error or the mean (SEM). Genes not regulated by RNAPII, including tRNA and snRNA genes as well as the majority of dubious ORFs were removed from the analysis.

Isolation of total RNA, Northern blotting and strand-specific multiplex RT-qPCR

Yeast strains were grown in YPD at 30°C until they reached an OD_{600} of 0.8. Total RNA was isolated using acid phenol extraction as described previously (19). RNA quality and quantity were assessed by UV spectroscopy using a NanoDrop 2000 (Thermo Scientific). Northern blotting and hybridization were done as described previously (20). 20 μg of total RNA were used to assess the cryptic transcript phenotype. Blots were exposed onto phosphorimaging screens and scanned using a Typhoon FLA9500.

For strand-specific RT-qPCR total RNA was treated with TURBO DNA-free DNase I (ThermoScientific) to remove genomic DNA according to the manufacturer's instructions. 3.5 μg of DNase-treated RNA were used for reverse transcription (RT) reactions containing 2 pmol of each gene-specific primer, 60 U of SuperScript III (ThermoScientific) and 0.3 μg of Actinomycin D (AppliChem) to prevent antisense cDNA artefacts. Two RT reactions containing 'forward' primers (Supplementary Table S3) annealing to antisense transcripts derived from target genes *VTH2* and *YEN1*, or *FAA2* and *ARO80* were set up. Each reaction also contained 2 pmol 'reverse' primer annealing to the canonical reference *ACT1* transcript. Annealing was done at 70°C for 10 minutes. First strand synthesis was performed at 55°C for one hour, followed by heat inactivation at 70°C for 15 min. All samples were quantitated by qPCR using PowerTrack SYBR Green Master Mix and a QuantStudio 5 Real-Time PCR System. Targets were first normalized to *ACT1*. Subsequently, results for mutant yeast strains were normalized to the mean signal for wildtype yeast samples using the comparative CT (ΔΔCT) method. Five biological replicates were performed for each strain.

RESULTS

The PWWP domain promotes binding of Ioc4 to nucleosomes *in vitro*

Previously, we found that localization and binding of Ioc4 to nucleosomes depend on Set2-mediated H3K36 trimethylation both *in vivo* and *in vitro* (8). Therefore, we wanted to assess the role and importance of the Ioc4 PWWP domain in this process in more detail.

First, we repeated our previous *in vitro* binding experiments using electromobility shift assays (EMSA) with some modifications. All binding assays were performed using nucleosomal core particles (NCPs) reconstituted onto 147 bp DNA fragments rather than mononucleosomes with DNA overhangs. Furthermore, we used a peptide ligation strategy to generate histone H3 containing uniformly unmethylated (me0) or trimethylated (me3) Lys36, which were subsequently used for histone octamer assembly and NCP reconstitution instead of chemically modified histone H3 (8). We also used a different Ioc4$_{\Delta PWWP}$ construct. Previously, we had based our Ioc4$_{\Delta PWWP}$ construct on the original annotation of the Ioc4 PWWP domain (7). However, this left part of the PWWP domain intact since the crystal structure reveals a much larger PWWP domain than anticipated (see below). Instead, we generated a new Ioc4$_{\Delta PWWP}$ construct with amino acids 1–178 deleted. The different experimental setups and Ioc4 constructs yield very comparable and reproducible results (Figure 1A, (8)). We find that full-length Ioc4 displays a slight but reproducible preference for trimethylated H3K36-containing nucleosome core particles when compared to unmethylated NCPs (Figure 1A–C). This preference for H3K36 trimethylated NCPs becomes more marked when we perform a competitive binding assay using differentially labeled nucleosomes (Figure 1C). Deletion of the PWWP domain (aa1–178) results in a considerable loss of binding of Ioc4$_{\Delta PWWP}$ to NCPs. Furthermore, Ioc4$_{\Delta PWWP}$ exhibits similar affinities towards unmethylated and trimethylated H3K36-containing nucleosome core particles (Figure 1A and B).

PWWP domain deletion results in reduced targeting of Isw1b *in vivo*

In wildtype cells Ioc4 localizes to the mid- to 3′-regions of ORFs that are characterized by high levels of H3K36 methylation as shown previously by us and others (Figure 1D) (8,21). In order to assess the contribution of the Ioc4 PWWP domain in correctly targeting Ioc4, and by inference Isw1b *in vivo*, we determined the localization of Ioc4 with and without its PWWP domain on a genome-wide level. Deletion of the Ioc4 PWWP domain does not interfere with protein folding as the mutant protein is still able to associate with Isw1 and Ioc2 to form Isw1b complex (Supplementary Figure S1A). Ioc4 without a functional PWWP domain (ΔPWWP) still localizes to ORFs. However, it does so at significantly reduced levels and loses the preference for mid- to 3′-ORF regions (Figure 1D). These more non-specific interactions are presumably mediated by other binding sites still present on the remaining Ioc4 molecule and/or interaction surfaces on the other complex subunits, such as the SANT and SLIDE domains of Isw1 (22). Taken together, these results clearly show that the Ioc4 PWWP domain promotes binding to nucleosomes *in vitro* as well as targeting Isw1b *in vivo*. Therefore, we set out to analyze the Ioc4 PWWP domain more closely and dissect its contributions to Isw1b function and chromatin association.

The Ioc4 PWWP domain preferentially binds trimethylated H3K36 nucleosomes *in vitro*

The PWWP domain alone also preferentially binds to H3K36me3-containing NCPs *in vitro* (Figure 1E–G). This preference is mediated by the aromatic cage in the PWWP domain (Supplementary Figure S2) and is abrogated by mutating the aromatic cage residue W22 to alanine. Similar observations have been made for other PWWP-containing proteins, such as human LEDGF, human BRPF1 or *S.p.* Hrp3 (23–25). Increased binding to the methylated over the unmethylated substrate is more apparent for the PWWP domain than for full-length Ioc4 (Figure 1B and F). This is due to the fact that the affinity towards NCPs is considerably lower for the PWWP domain alone than that for full-length Ioc4, in agreement with our finding that the remaining Ioc4 protein contributes to nucleosome binding both *in vivo* and *in vitro* (Figure 1B and D).

The Ioc4 PWWP structure reveals highly charged patches and a unique insertion motif

In order to further our understanding of the Ioc4 PWWP domain we solved the crystal structure of the Ioc4 PWWP domain at 2.3 Å (Figure 1H, Supplementary Table S2). Analysis of the structure showed a high degree of structural conservation overall when compared to other PWWP domains. Overlay of the PWWP domains of Ioc4 and BRPF1 confirmed the high degree of conservation of PWWP domains at both, a structural (Supplementary Figure S3A)

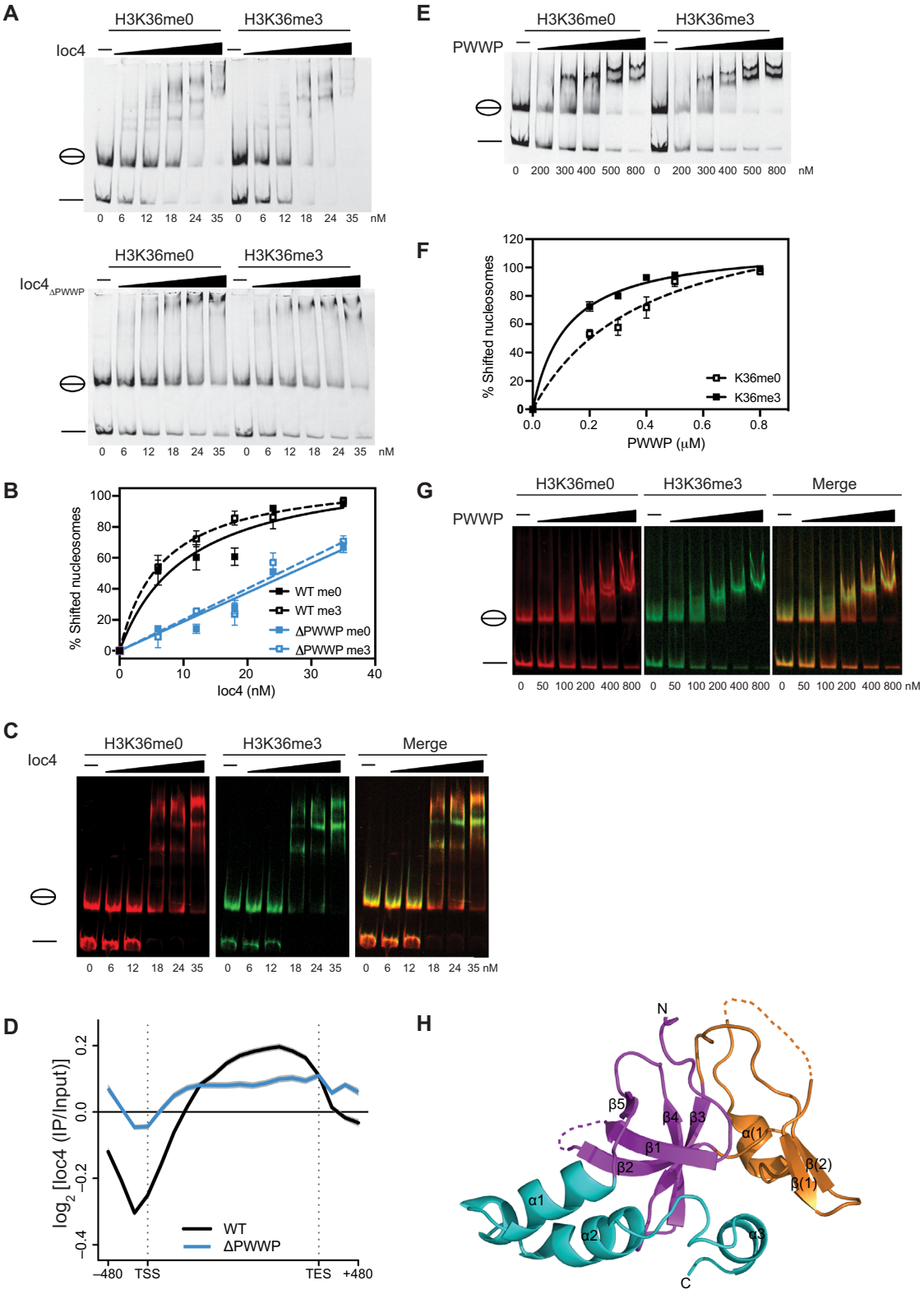

Figure 1. Functional Ioc4$_{PWWP}$ is promotes chromatin binding *in vivo* and *in vitro*. (**A**) EMSA analysis of full-length, wildtype Ioc4 and Ioc4$_{\Delta PWWP}$ binding to NCPs containing either unmethylated or trimethylated histone H3K36. (**B**) Quantitation of EMSAs shown in (A). (**C**) Competitive EMSA (cEMSA) analysis of full length, wildtype Ioc4 binding to unmethylated (red) and trimethylated (green) H3K36 NCPs. (**D**) Metagene analysis ($n = 6451$ genes) of ChIP-chip data using yeast genome tiling arrays for wildtype (WT) Ioc4 and Ioc4$_{\Delta PWWP}$. The transcription start (TSS) and end sites (TES) are indicated. (**E**) EMSA analysis of wildtype PWWP domain binding to NCPs containing either unmethylated or trimethylated histone H3K36. (**F**) Quantitation of EMSAs shown in (E). (**G**) Competitive EMSA (cEMSA) analysis of wildtype PWWP binding to unmethylated (red) and trimethylated (green) H3K36 NCPs. (**H**) Crystal structure of the Ioc4 PWWP domain. The insertion motif between β2 and β3 is shown in orange.

and sequence level (Supplementary Figure S3B). In common with other PWWP domains the Ioc4 PWWP domain contains a highly conserved, antiparallel, five-stranded β-barrel at its N-terminus. The α-helical composition at the C-terminus of the domain is also maintained, although the number and precise spatial relationship to the rest of the domain can vary in individual PWWP domains (3). A unique feature of the Ioc4 PWWP domain is the presence of an exceptionally long insertion motif (aa 27–110). Other PWWP domain-containing proteins have either no (e.g. LEDGF) or a much shorter (e.g. BRPF1) insertion motif (3,26).

Close analysis of the Ioc4 PWWP domain crystal structure revealed the presence of one acidic and two basic patches (Figure 2A). PWWP domains were initially identified as DNA-binding domains and several PWWP domains have been shown to bind to double-stranded DNA (23,27–30). Given this charge distribution on the Ioc4 PWWP domain we hypothesized that it may be able to bind histones and DNA directly via the acidic and basic patches, respectively. Using pull-down assays we could show that the Ioc4 PWWP domain interacts both with histone octamers (Figure 2C) and histone H3/H4 tetramers (Supplementary Figure S4A). In both cases full-length Ioc4 displays higher affinity towards histones compared to the PWWP domain alone.

The Ioc4 PWWP domain binds single and double stranded nucleic acids

Next we investigated binding of the PWWP domain to DNA. Using EMSAs we could show that the Ioc4 PWWP domain can indeed bind to DNA (Figure 2D). Since most PWWP domains do not exhibit sequence specificity (26) and are thought to interact with the negatively charged phosphate backbone we also tested binding of the domain to double-stranded (ds) RNA and RNA:DNA hybrid molecules. The PWWP domain bound both dsDNA and DNA:RNA hybrid molecules equally well, but displayed lower affinity towards dsRNA (Figure 2D). The GC content does not seem to affect binding since both substrates are bound at equal levels (Supplementary Figure S4C). We then also tested binding of the PWWP domain to single-stranded (ss) DNA and RNA. Again it bound both molecules, but displayed higher affinity for ssRNA (Figure 2E). Notably, the affinity of the Ioc4 PWWP domain for dsDNA is similar to that for ssRNA (Table 1). Whether this finding has functional implications for Isw1b is unclear at present. Interestingly, previous UV cross-linking experiments showed that both Isw1 and Ioc2 interact with RNA *in vivo* (31). Overall, the PWWP domain binds H3K36 trimethylated nucleosome core particles with ca. 6-fold higher affinity compared to dsDNA, suggesting that H3K36 trimethylation, histone and DNA binding are all important for the interaction of the PWWP domain with nucleosomes.

We also tested interaction of full-length Ioc4 with nucleic acids. Overall, Ioc4 has a much higher affinity for all substrates when compared to the PWWP domain alone. However, the differences in affinity of Ioc4 for dsDNA and dsRNA are smaller (Figure 2F). The same applies to Ioc4 binding to ssRNA and ssDNA (Figure 2G).

Nucleosome binding by $Ioc4_{PWWP}$ requires interaction with DNA

The basic patches apparent on the Ioc4 PWWP domain consist of a series of lysine and arginine residues (Figure 2B). We chose several surface residues to generate site mutants. We then tested the ability of the mutant proteins to bind DNA. While the wildtype PWWP protein associated with DNA, most mutants did not bind DNA *in vitro* (Supplementary Figure S4D). We then tested the binding behaviour of a PWWP domain containing K149E K150E (2KE) mutations in more detail. The 2KE mutant was completely unable to bind double-stranded DNA (Figure 3A and B).

Next, we tested the ability of DNA-binding deficient PWWP domain to associate with nucleosomes. Surprisingly, the $PWWP_{2KE}$ mutant exhibited no interaction with nucleosome core particles *in vitro* (Figure 3C and D). These results suggest that DNA binding is essential in mediating the stable interaction of the Ioc4 PWWP domain with nucleosomes. Mutating K149 and K150 to alanine instead of lysine results in the same loss of binding of the mutant $PWWP_{2KA}$ domain to both DNA and nucleosomes (Supplementary Figure S4E and F).

The full-length $Ioc4_{2KE}$ mutant shows reduced binding of DNA and NCPs *in vitro*

We also tested the effects of the 2KE mutant in the context of the full-length Ioc4 protein. While the mutant displays some affinity towards DNA, the binding profile of $Ioc4_{2KE}$ to DNA is virtually identical to that of $Ioc4_{\Delta PWWP}$ (Figure 3E, F and K). Also, $Ioc4_{2KE}$ does bind to nucleosome core particles, however it does so at much reduced levels (Figure 3G and H). Furthermore, it can no longer distinguish between unmethylated and trimethylated H3K36-containing NCPs, in a manner similar to $Ioc4_{\Delta PWWP}$ (Figure 1A and B), suggesting that the mutation of these two lysine residues is sufficient to reduce nucleosome binding of the PWWP domain even in the context of the full-length protein. The residual association of $Ioc4_{2KE}$ with NCPs is therefore likely mediated by regions of the Ioc4 protein outside of the PWWP domain.

Two previous studies investigating the structure of the human LEDGF PWWP domain also showed the ability of this domain to bind DNA (23,24). PWWP domains in other proteins such as Pdp1, Hrp3, HDGF, MSH6, ZMYND11 and murine Dnmt3b were also shown to bind DNA (23–25,27–29). Thus, it seems the ability of PWWP domains to bind DNA is a conserved feature of PWWP domains in general. However, in contrast to our results, van Nuland and co-workers (23) found that most mutations interfering with DNA binding reduced, but did not completely abolish nucleosome binding by the LEDGF-PWWP. A further difference between the PWWP domains from Ioc4 and LEDGF is the fact that some LEDGF-PWWP DNA-binding mutants still retain their preference for H3K36-methylated nucleosomes, while the Ioc4 $PWWP_{2KE}$ mutant does not bind to nucleosomes at all, irrespective of its H3K36 methylation status, while the full-length $Ioc4_{2KE}$ mutant binds both types of NCPs equally well (Figure 3G, H, Supplementary Figure S4G). Only the wildtype PWWP domain or the

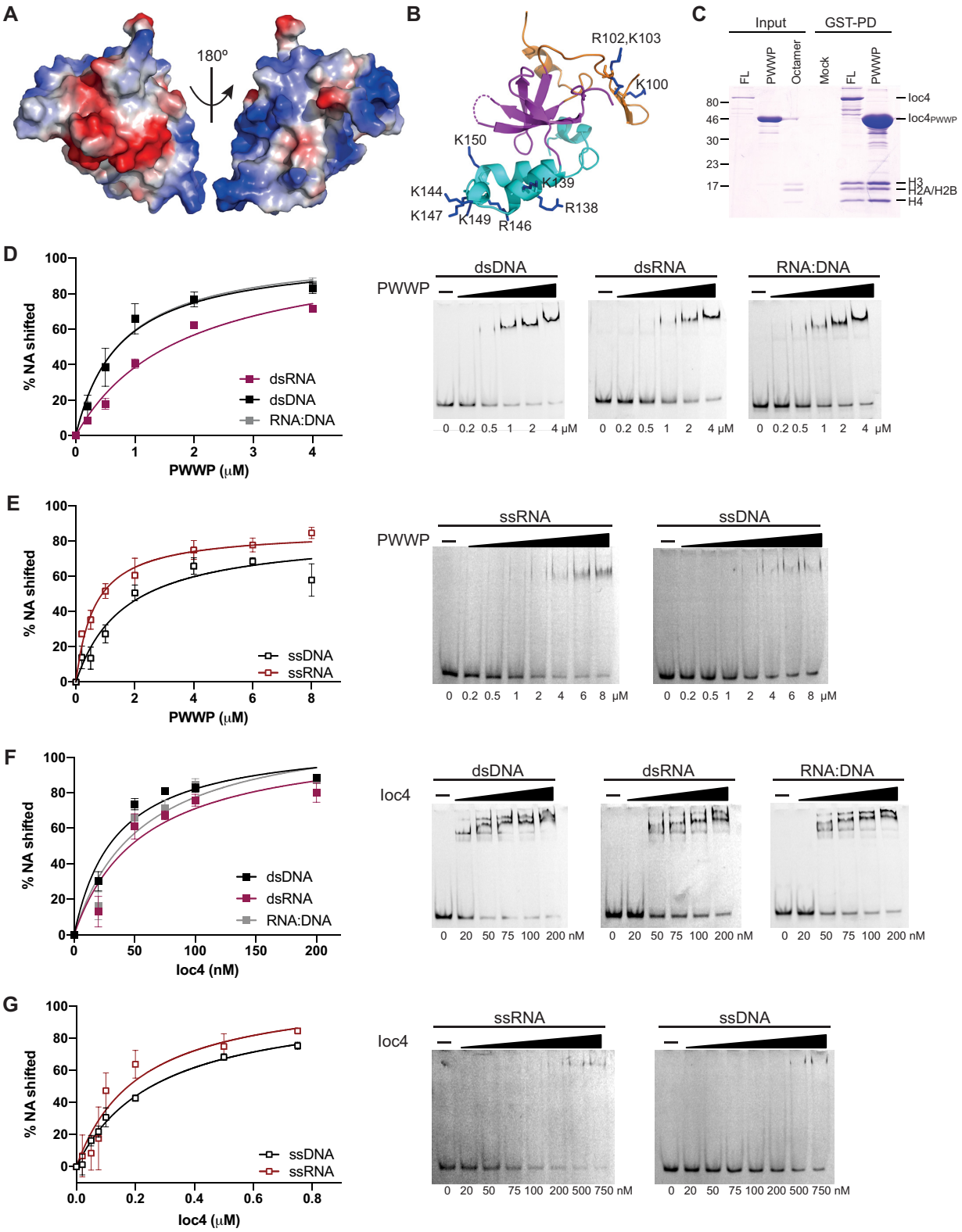

Figure 2. The Ioc4 PWWP domain binds double-stranded and single-stranded nucleic acids. (**A**) Electrostatic surface of the Ioc4 PWWP domain. Negative, positive and neutral charges are shown in red, blue and white, respectively. (**B**) Lysine and arginine residues contributing to the basic patches. All residues indicated were mutated and tested for DNA binding (Supplementary Figure S4D). (**C**) Pull-down assay of GST-tagged Ioc4 proteins with core histone octamers. (**D–G**) EMSA analyses of the wildtype PWWP domain (D, E) or full-length Ioc4 (F, G) binding to double stranded (D, F) or single stranded (E, G) nucleic acids.

Table 1. Binding parameters. The protein construct or complex is indicated. Nucleic acid substrates include single-stranded (ss) and double-stranded (ds) RNA, DNA, RNA:DNA hybrid molecules or nucleosomal core particles (NCP). Apparent dissociation constants (K_D) are indicated if determined, including the 90% confidence interval (CI) and goodness of fit (R^2)

	PWWP			Isw1b			Ioc4			$Ioc4_{\Delta PWWP}$			$Ioc4_{2KE}$		
	K_D (μM)	CI	R^2	K_D (nM)	CI	R^2	K_D (nM)	CI	R^2	K_D (nM)	CI	R^2	K_D (nM)	CI	R^2
dsDNA	0.81	(0.37; 1.51)	0.884				34	(27; 44)	0.906	121	(79; 192)	0.942	76	(43; 134)	0.892
RNA:DNA	0.76	(0.66; 0.88)	0.977				55	(34; 87)	0.906						
dsRNA	1.80	(1.37; 2.40)	0.973				56	(32; 97)	0.877						
ssDNA	1.65	(1.17; 2.32)	0.869				275	(206; 376)	0.953						
ssRNA	0.64	(0.49; 0.84)	0.914				213	(111; 448)	0.756						
NCP unmodified	0.45	(0.28; 0.69)	0.924												
NCP H3K36me0	0.40	(0.25; 0.95)	0.947	*57.3*	*Ambiguous*	0.817	11	(5.0; 23)	0.876						
NCP H3K36me3	0.12	(0.10; 0.15)	0.992	4.8	(2.8;8.0)	0.895	6.7	(4.5; 9.7)	0.958						

full-length Ioc4 protein can achieve this distinction. In part these differences may also be attributable to the fact that the authors used GST-fusion proteins for their EMSAs, which can dimerize through the GST tag and thus provide a second binding site, thereby increasing its affinity, while we used proteins containing monomeric MBP- or His-tags.

The insertion motif promotes binding to nucleosomes, histones and DNA

Since the Ioc4 PWWP domain contains a unique insertion motif (INS) that is either completely absent or much shorter in all other PWWP domains studied so far, we sought to investigate its contributions towards Ioc4 PWWP functions. Therefore, we generated a PWWP mutant that lacks most of the insertion motif (Δ43–105, ΔINS). Residues for deletion were chosen to minimize potential deleterious effects on the folding of the mutant PWWP domain. Circular dichroism and/or nano-differential scanning fluorimetry (nano-DSF) showed that all purified, recombinant PWWP and Ioc4 proteins were indeed folded (Supplementary Figure S1B–D). Also, deletion of the insertion motif within the *IOC4* gene in yeast still allows for the successful purification of the mutant $Isw1b_{\Delta INS}$ remodeller, a further indication that the mutant protein is able to fold correctly and does not interfere with the binding of the Isw1 and Ioc2 subunits (Supplementary Figure S1A).

First, we tested binding of $PWWP_{\Delta INS}$ to nucleosome core particles. In contrast to the wildtype PWWP domain, deletion of the insertion motif largely abrogates stable interactions with NCPs (Figure 3J), suggesting the insertion motif stabilizes contacts between the PWWP domain and nucleosomes. Analysis of the amino acid composition of the insertion motif reveals the presence of a series of negatively charged amino acids, suggesting a potential role in histone binding. Indeed, a $PWWP_{\Delta INS}$ mutant does not bind histones at all, while the insertion motif by itself still associates with histones (Supplementary Figure S4A and B). The insertion motif also contributes several residues towards one of the basic patches seen in the crystal structure. Therefore, we also tested the ability of $PWWP_{\Delta INS}$ to bind to DNA. Unlike the wildtype domain, the $PWWP_{\Delta INS}$ mutant is not able to form a stable complex with dsDNA, although it may form transient interactions at very low levels as evidenced by increased smearing of the DNA band at higher protein concentrations (Figure 3I).

The Ioc4 PWWP domain binds across DNA gyres

The effects of the $PWWP_{2KE}$ and $PWWP_{\Delta INS}$ mutants can be explained by modeling our structure of the Ioc4 PWWP domain onto the recently published cryo-EM structure determined for the human LEDGF-PWWP domain bound to a nucleosome (Figure 3L, Supplementary Figure S5) (32). We see a high degree of overlap, especially over the highly conserved beta barrel. Binding of the Ioc4 PWWP domain also occurs across DNA gyres and is mediated by the basic patch seen in Figure 2A. Residues K149 and K150 are in close contact with the DNA sugar phosphate backbone which explains why their replacement completely abrogates DNA and nucleosome binding. Similarly, the insertion motif is in close contact with one of the nucleosomal DNA

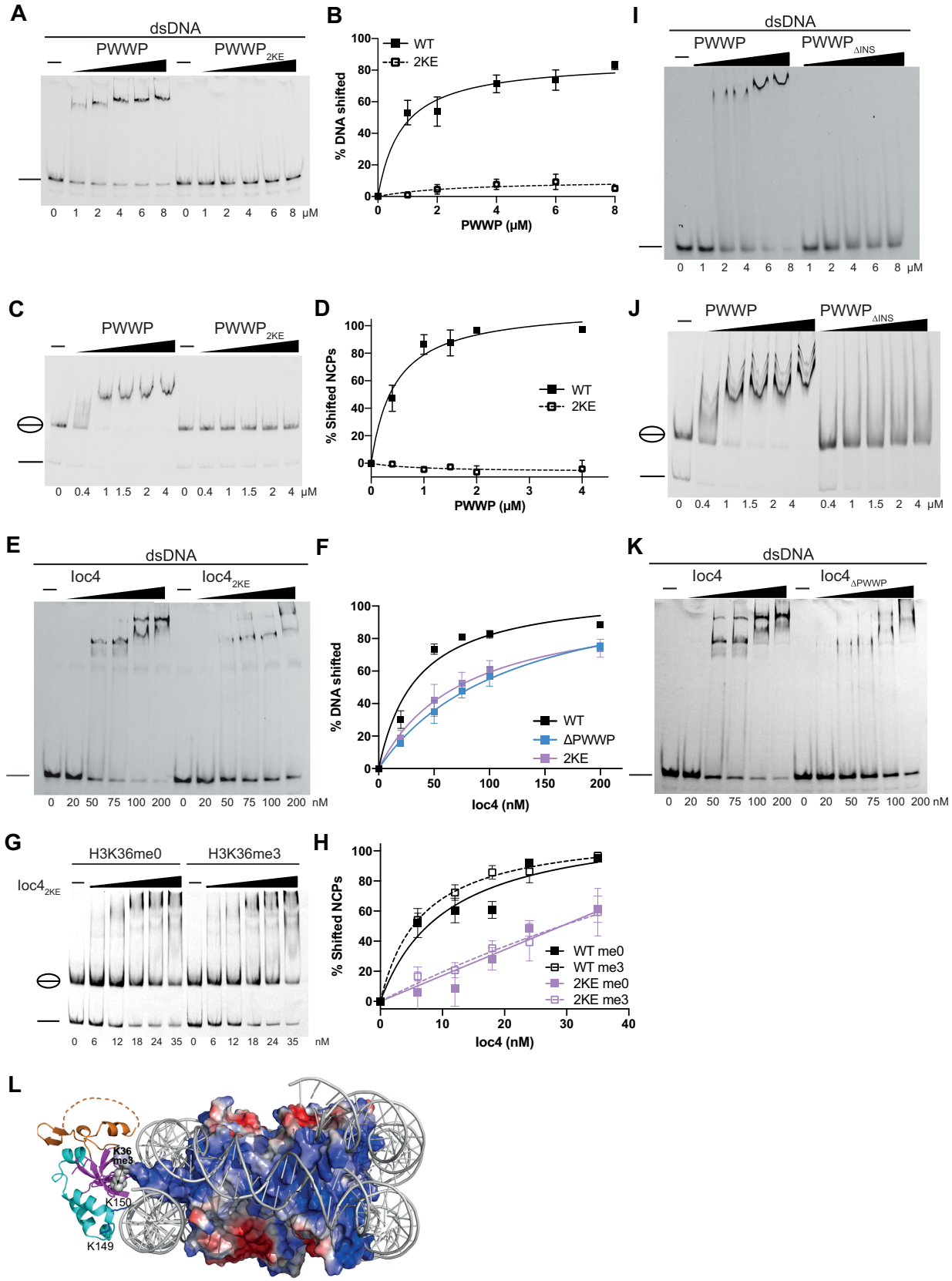

Figure 3. DNA-binding by $Ioc4_{PWWP}$ promotes its interaction with nucleosomes. (**A–D,I, J**) EMSA analyses of wildtype PWWP, the $PWWP_{2KE}$ and $PWWP_{\Delta INS}$ mutants.(A, C, I, J) binding to double stranded DNA (A, I) or NCPs (C, J). Quantitations of triplicate experiments are shown in (B, D). (**E–H, K**) EMSA analyses of full-length Ioc4, the $Ioc4_{2KE}$ and $Ioc4_{\Delta PWWP}$ mutants (E,K,G) binding to double stranded DNA (E,K) or NCPs (G). Quantitations of triplicate experiments are shown in (F, H). (**L**) Model of Ioc4 PWWP binding to NCP. Homology model based on Wang *et al*. (32).

gyres, thus potentially stabilizing the interactions between the PWWP domain and the nucleosome core particle. While the stretch of negatively charged residues within the insertion motif is not resolved in the crystal structure, it seems likely that it interacts with the positively charged histone tails and thereby provides further stabilization of the interaction. A second set of positively charged residues within the insertion motif points away from the NCP surface and may contribute towards the binding of linker DNA and/or the DNA associated with neighbouring nucleosomes (Supplementary Figure S5).

Targeting of Ioc4 *in vivo* depends on H3K36 methylation and DNA binding

The results from our *in vitro* experiments suggest that both the insertion domain and DNA binding by the Ioc4 PWWP domain promote stable interactions with DNA, histones and nucleosomes. Therefore, we wanted to test how these features influence the localization of Ioc4 *in vivo.* To assess the effects of these mutations *in vivo*, we generated full-length, 3xFLAG-tagged Ioc4 yeast strains carrying either the K149E K150E (2KE) mutation or the insertion motif deletion (ΔINS). Furthermore, we wanted to compare the localization of these Ioc4 mutants to the recruitment deficiencies of wildtype Ioc4 in a *set2*Δ background that contains no H3K36 methylation, as well as a yeast strain with the entire PWWP domain deleted (ΔPWWP). Finally, we assessed the impact of the PWWP aromatic cage directly by mutating W22 to alanine. Neither deletion of the PWWP domain nor the mutations of K149/K150 and/or W22 affected Ioc4 protein expression or stability when compared to the wildtype protein (Supplementary Figure S6A).

We then determined the genome-wide localization of Ioc4 in a *set2*Δ background as well as of the $Ioc4_{2KE}$ and $Ioc4_{\Delta INS}$ mutants, and compared these to the localization patterns of wildtype Ioc4. In the absence of H3K36 methylation (*set2*Δ) we saw reduced targeting of Ioc4 specifically to mid- and 3′-ORFs, in a manner comparable to the deletion of the entire Ioc4 PWWP domain (Figure 4A, B, Supplementary Figure S6B). Some non-specific background binding of Ioc4 remained in the *set2*Δ mutant. The aromatic cage mutant $Ioc4_{W22A}$ which is unable to distinguish un- and trimethylated H3K36 nucleosomes displayed a similar reduction in ORF localization when tested by ChIP-qPCR (Figure 4C, Supplementary Figure S6C). The $Ioc4_{2KE}$ mutation also resulted in reduced targeting of Ioc4 to mid- and 3′-ORFs, in a manner almost identical to that of Ioc4 localization in a *set2*Δ mutant and comparable to the deletion of the entire Ioc4 PWWP domain (Figure 4A–C, Supplementary Figure S6B). The background binding seen in all mutants is consistent with the presence of other interaction surfaces remaining both within the PWWP domain as well as on the remainder of the Ioc4 protein, in agreement with our *in vitro* binding assays. Furthermore, additional binding interfaces present within Isw1b on Ioc2 and/or Isw1 could also contribute to recruitment *in vivo*. Similarly, *in vitro* binding assays of purified Isw1b remodeler show preferential binding of H3K36me3-containing nucleosomes, yet can still interact with unmethylated nucleosomes albeit with lower affinity (Figure 4D). We also tested whether Ioc4 interaction with methylated H3K36 and simultaneous DNA binding display additive effects with regards to Ioc4 localization by generating an $Ioc4_{W22A\ 2KE}$ double mutant. Using ChIP-qPCR we see no further reduction in chromatin association of the double mutant when compared to the single mutants (Figure 4C). Taken together, these results suggest that both recognition of H3K36 methylation via the aromatic cage as well as the ability of the Ioc4 PWWP domain to bind DNA are each necessary for the correct targeting of Ioc4 and consequently of Isw1b *in vivo*.

Deletion of the insertion motif alone had little overall effect on the genome-wide Ioc4 localization over ORFs *in vivo* (Supplementary Figure S6D). Interestingly, a closer look at the data reveals that deletion of the Ioc4 insertion motif has opposite effects on $Ioc4_{\Delta INS}$ localization for different categories of genes. While less $Ioc4_{\Delta INS}$ is found over shorter genes, increased levels of $Ioc4_{\Delta INS}$ are observed over the ORFs of genes longer than 1000 bp (Figure 4E, Supplementary Figure S6E), suggesting multiple recruitment mechanisms may be at play for different categories of genes. Longer genes generally display more extensive domains of H3K36 trimethylation since the Set2 methyltransferase is recruited to RNAPII phosphorylated on Ser2 of its C-terminal domain (CTD). Furthermore, Set2 as well as H3K36me3 signals are mostly found over genes beyond 400 bp from the transcription start site (33,34). Indeed, looking at H3K36me3 levels in these same gene groups, we see that they are only enriched for genes longer than 1000 bp (Figure 4F). Accordingly, loss of H3K36 trimethylation in a *set2*Δ mutant leads to reduced Ioc4 localization precisely over this group of genes (Figure 4E). Similarly, deletion of the Ioc4 PWWP domain leads to a similar reduction of $Ioc4_{\Delta PWWP}$ over the same set of genes (Figure 4E). Deletion of the insertion motif leads to a significant reduction in PWWP binding to histones and nucleosomes *in vitro* (Figure 3J, Supplementary Figure S4A). In contrast, deletion of the insertion motif in the context of full-length Ioc4 leads to a significant change in its binding behavior towards nucleosome core particles *in vitro*, resulting in the more prominent association of multiple copies of the mutant Ioc4 protein with NCPs when compared to the wildtype protein (Supplementary Figure S4I). It is possible that this is also reflected in the increased $Ioc4_{\Delta INS}$ association *in vivo* with the H3K36 trimethylated, nucleosome-packed ORFs over longer genes that are only partially disassembled during transcription. In contrast, the group of genes shorter than 1000 bp contains many highly active genes characterized by poorly organized chromatin where nucleosomes are more likely to be completely displaced from the DNA (35–38).

Reduced targeting of Ioc4 results in growth defects and non-coding transcription

To assess the importance of functional Isw1b remodeler *in vivo* we used growth assays to investigate the impact of our mutants. Deletion of *IOC4* leads to reduced growth on media containing propiconazole, a fungicide that impairs ergosterol biosynthesis (39). Deletion of the Ioc4 PWWP domain leads to a similar growth defect as for *ioc4*Δ. Also, the aromatic cage mutant $IOC4_{W22A}$ and the DNA-binding deficient $IOC4_{2KE}$ exhibit slow growth phenotypes which are

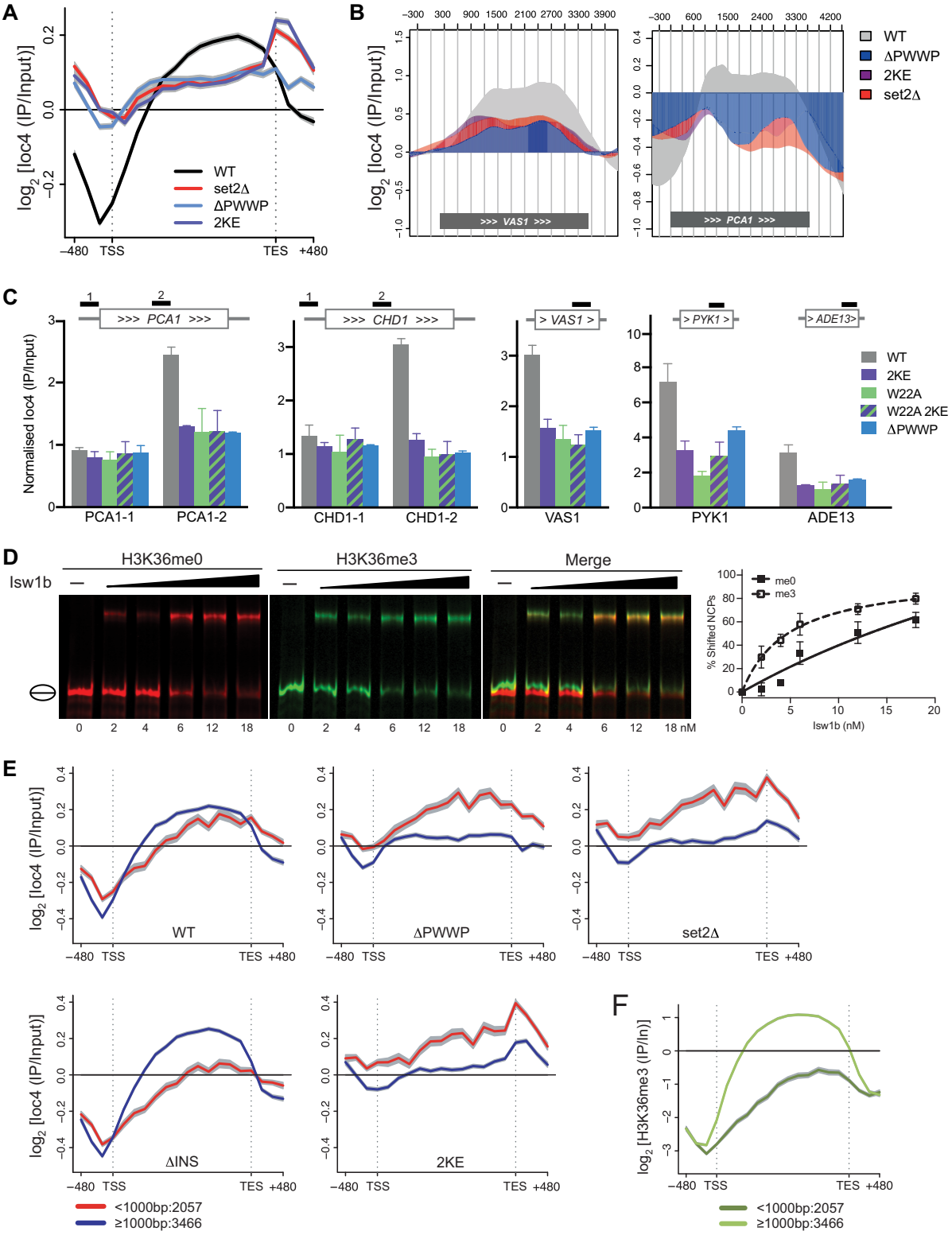

Figure 4. Ioc4 recruitment depends on binding to DNA and H3K36 methylation. (**A**) Metagene analysis of ChIP-chip experiments using yeast genome tiling arrays. Whole-genome average data ($n = 6451$ genes) for three independent experiment were plotted as mean ± s.e.m. (gray) for full-length Ioc4 in wildtype (WT) and *set2*Δ backgrounds as well as Ioc4 without its PWWP domain (ΔPWWP) and the DNA-binding mutant $Ioc4_{2KE}$. (**B**) Localization of wildtype and mutant Ioc4 over individual genes. (**C**) ChIP-qPCR analysis of wildtype Ioc4, $Ioc4_{\Delta PWWP}$, the DNA-binding mutant $Ioc4_{2KE}$, the aromatic cage mutant $Ioc4_{W22A}$ and the double mutant $Ioc4_{W22A\ 2KE}$. Three biological replicates were analyzed and plotted as mean ± s.e.m. (**D**) cEMSA analysis of Isw1b binding to unmethylated (red) and trimethylated (green) H3K36 NCPs. (**E-F**) Metagene analysis of wildtype and mutant Ioc4 (**E**) and H3K36me3 (**F**) localization using ChIP-chip experiments and yeast genome tiling arrays. Whole-genome average data for three independent experiment were plotted as mean ± s.e.m. (gray) for genes clustered according to gene length. The number of genes in each group is indicated.

not further exacerbated in the *IOC4*$_{W22A\ 2KE}$ double mutant (Figure 5A).

Previous work has shown that functional Isw1b remodeler is necessary for the retention of existing histones over ORFs. Deletion of *IOC4* or *ISW1* leads to increased incorporation of soluble histones and disrupts chromatin organization over ORFs, which in turn results in the exposure of cryptic promoters and the production of non-coding transcripts (8). Since our results suggested that the ability of the Ioc4 PWWP domain to bind nucleosomal DNA and/or to associate with methylated H3K36 is important for its recruitment, we wanted to determine whether reduced localization of Ioc4 and Isw1b over ORFs also results in non-coding transcription. We used *STE11*, a well-characterized cryptic transcript model gene to assess the impact of our different *IOC4* mutants. Deletion of *IOC4* alone does not produce a cryptic transcript phenotype discernible by Northern blotting. However, it has been shown previously that deletion of *ISW1* and *CHD1* has additive effects with respect to cryptic transcription (8,40). Hence, we investigated the effects of various *IOC4* mutants on cryptic transcription in a *chd1*Δ background. While the overall levels of cryptic transcripts were relatively low, we observed similar and reproducible levels of the small cryptic *STE11* transcript for *ioc4*Δ, the *IOC4*$_{2KE}$ as well as the *IOC4*Δ_{PWWP} mutants in a *chd1*Δ background (Figure 5B). These results confirm that Isw1b activity in these *IOC4* mutants is reduced *in vivo*, consistent with the lower levels of mutant Ioc4 chromatin association observed. Deletion of the insertion motif leads to a minimal effect on cryptic transcription only detectable at high contrast. However, recruitment of Ioc4$_{\Delta INS}$ to *STE11* is unchanged relative to wildtype Ioc4, suggesting that increased cryptic transcription is unlikely to occur in this context.

Furthermore, we developed a new, strand-specific, multiplex RT-qPCR approach to assess the levels of antisense transcription over several genes. Candidate genes were identified from RNA-seq data obtained for *isw1*Δ. The levels of antisense (as) transcripts produced in different *IOC4* mutants were determined in either a wildtype or *chd1*Δ background (Figure 5C and D). Chd1 has no effect on antisense transcription over the *FAA2* and *ARO80* genes. Deletion of the PWWP domain, the absence of the aromatic cage (W22A) or DNA-binding (2KE) all resulted in the production of antisense transcripts when compared to wildtype yeast (Figure 5D). Double deletion of *IOC4* and *CHD1* shows large additive effects on antisense transcription over *YEN1* and *VTH2*. However, deletion of the PWWP domain as well as the 2KE and W22A mutants all display upregulated levels of antisense transcripts when compared to *chd1*Δ alone (Figure 5C). The relative effects of the 2KE and W22A mutations vary depending on the asRNA investigated. With the exception of *FAA2* the effects of these two mutations are not additive, in agreement with our other *in vivo* data on growth and Ioc4 localization.

Ioc4 PWWP domain contributes to efficient nucleosome sliding by Isw1b

We have shown previously that cryptic transcription occurs in catalytically inactive Isw1 mutants, indicating that remodeling activity is required to suppress this phenotype (8). The *in vivo* results in this study show that a functional Ioc4 PWWP domain is needed for correct targeting of the Isw1b remodeler and promotes suppression of non-coding transcription. We therefore wanted to test whether the Ioc4 PWWP domain is needed primarily only for the correct targeting of Isw1b remodelers to ORFs, or whether it also affects Isw1b remodeling activity directly. Therefore, we purified wildtype and mutant Isw1b remodelers from yeast cells via TAP-tagged Ioc4 subunits (Supplementary Figure S1A) and tested their remodeling activities *in vitro* using methyllysine analogue (MLA) H3K36Cme3-containing nucleosomes (Figure 6). MLA nucleosomes were used for the remodeling assays because the peptide-ligated variety used for all other *in vitro* assays tended to disassemble during remodeling reactions, possibly due to the fact that peptide ligation required mutagenesis of T45 in histone H3 which is near the nucleosome dyad axis. Wildtype Isw1b preferentially moves histone octamers from a central position towards the ends of the DNA (41). Remodeler with its entire Ioc4 PWWP domain deleted (Isw1b$_{\Delta PWWP}$), as well as Isw1b containing the DNA-binding deficient Ioc4$_{2KE}$ or the aromatic cage mutant Ioc4$_{W22A}$ all exhibit reduced remodeling activities compared to wildtype Isw1b, although this is most apparent for the W22A mutants which displays barely any activity at all (Figure 6A–E). It is not entirely clear why the aromatic cage mutant has a larger effect than deletion of the entire PWWP domain itself, especially since the W22A site mutation does not interfere with PWWP domain folding (Supplementary Figure S1D) or purification of the mutant remodeling complex (Supplementary Figure S1A). These results clearly show that a functional PWWP domain in Ioc4 promotes full Isw1b remodeler function.

While deletion of the insertion motif affects the interactions of the PWWP with DNA, histones and nucleosomes *in vitro*, it had very little effect on the remodeling activity of Ioc4$_{\Delta INS}$-containing Isw1b (Figure 6D and E). These results suggest that the mutant Isw1b$_{\Delta INS}$ is able to fulfill remodeler functions *in vivo* in a manner similar to the wildtype, although the insertion motif has a contributory role in remodeler recruitment.

DISCUSSION

Here, we report the crystal structure of the Ioc4 PWWP domain as well as a detailed analysis of its binding preferences. We have analyzed the PWWP domain on its own as well as in the context of the full-length Ioc4 protein and the entire Isw1b chromatin remodeler, both *in vitro* and *in vivo* (Figure 6F).

The crystal structure of the Ioc4 PWWP domain exhibits two interesting features that help us understand its biological function. In addition to the preferential binding of the Ioc4 PWWP domain to H3K36 trimethylated nucleosomes via its aromatic cage (Figure 1, Supplementary Figure S2), its basic patches are important for interactions with DNA (Figures 2 and 3). Mutations within these basic patches lead to a complete loss of DNA and nucleosome binding. Interactions of PWWP domains with DNA have been described also for the PWWP domains of other proteins such as the human LEDGF, DNMT3b and MSH6 proteins as well as

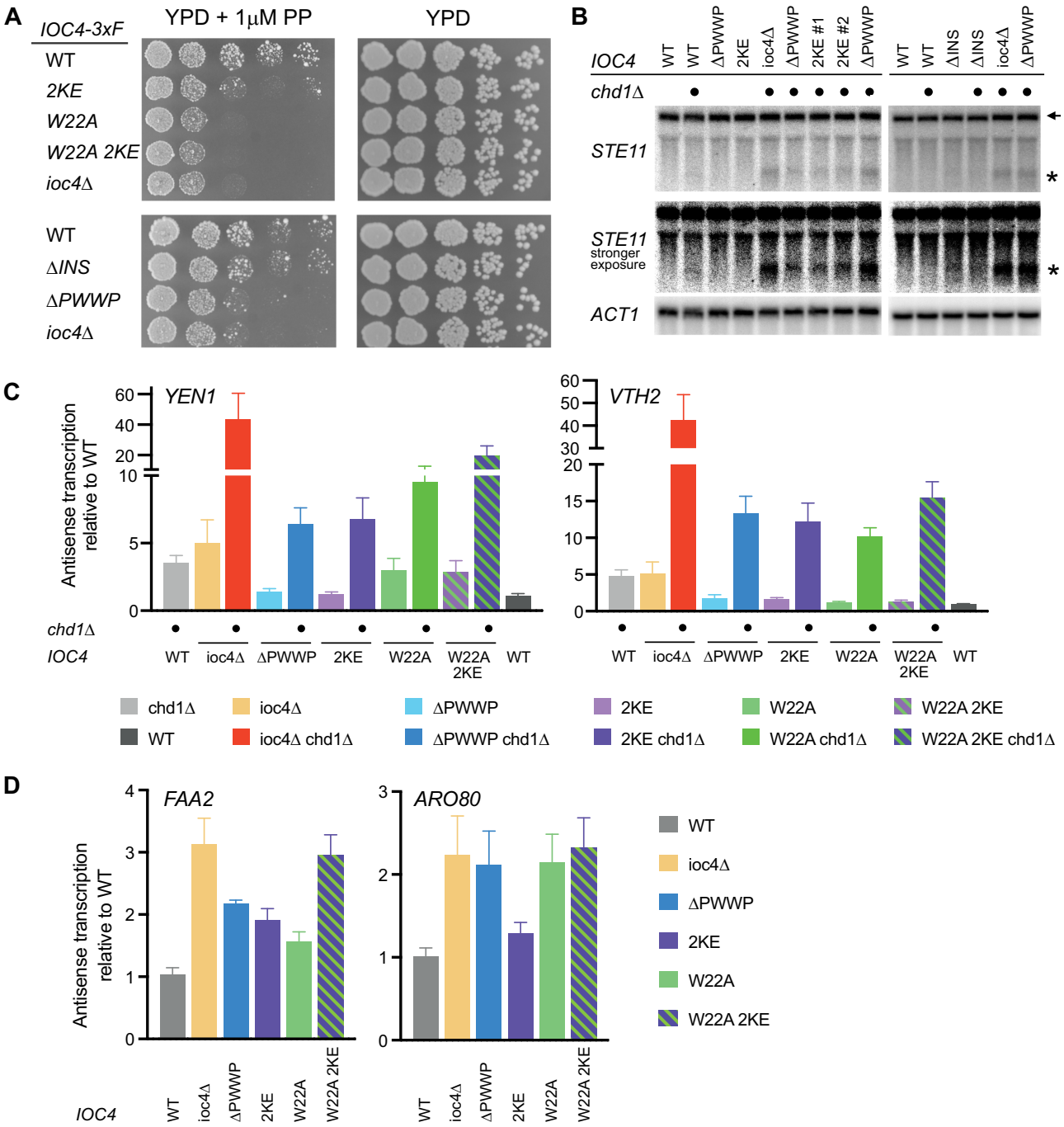

Figure 5. Full remodeler functions and suppression of cryptic transcription depend on Ioc4$_{PWWP}$. (**A**) Wildtype and mutant yeast strains were grown at 30°C on YPD ± 1 μM propiconazole. (**B**) Northern blot of total RNA to investigate cryptic transcription. A probe directed against the 3′ end of *STE11* was used. *ACT1* was used as a loading control. The additional deletion of *CHD1* is indicated. The full-length (←) and short cryptic (*) transcripts are indicated. A stronger exposure better reveals the rise of cryptic transcripts in the mutants. (**C, D**) Strand-specific, multiplex RT-qPCR was used to determine the levels of antisense transcription in wildtype yeast and different *IOC4* mutants. The additional deletion of *CHD1* in (C) is indicated. Five independent experiments were performed and plotted as mean ± s.e.m.

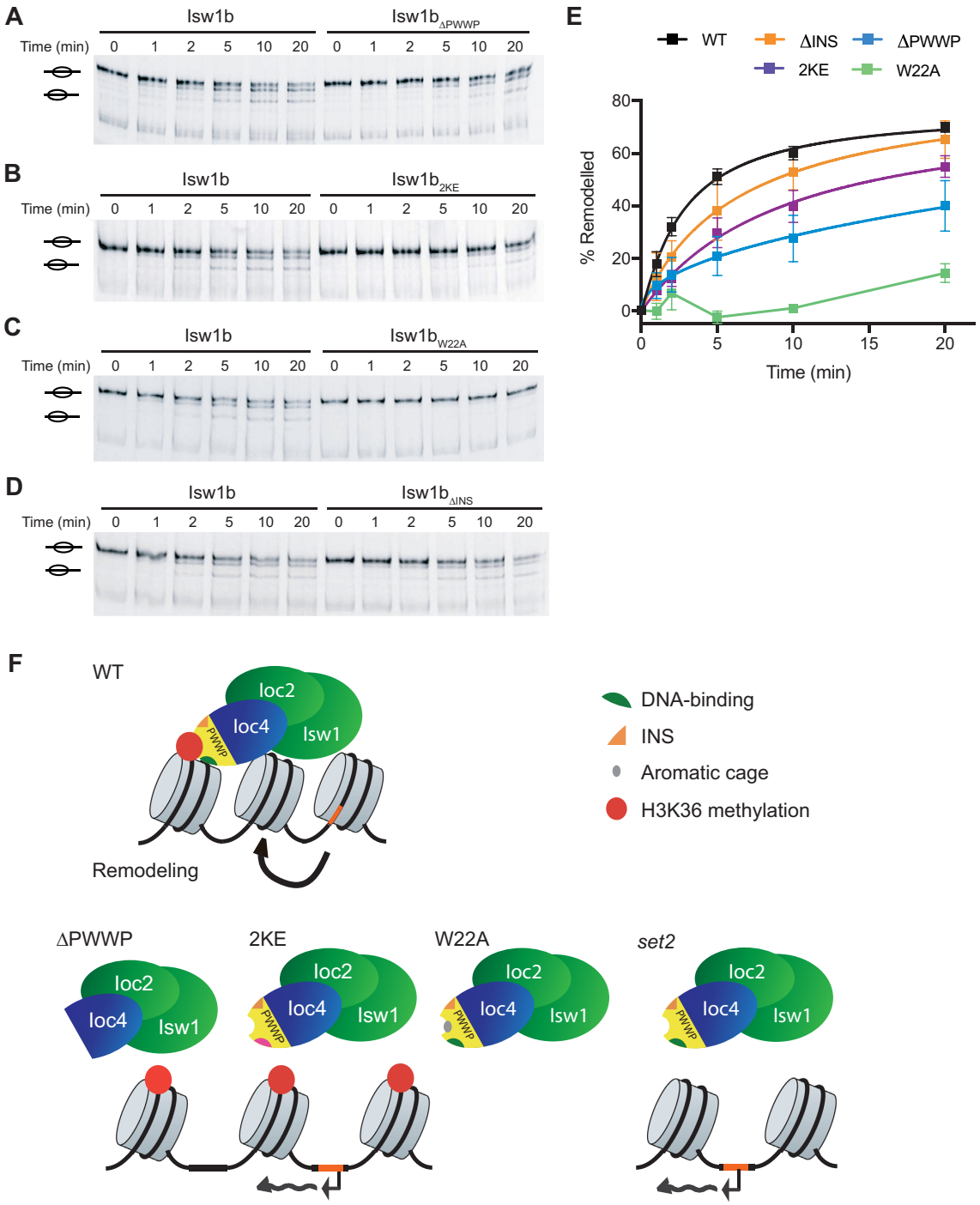

Figure 6. The intact Ioc4 PWWP domain promotes remodeling by Isw1b. (**A–D**) Sliding assays of wildtype and mutant Isw1b remodelers lacking the Ioc4 PWWP domain (A), containing the 2KE (B) or W22A (C) site mutations, or lacking the insertion motif (D). Centrally positioned, MLA-K36$_C$me3-containing mononucleosomes were remodeled by the addition of remodeler for up to 20 min. Center and side positioned nucleosomes are indicated. (**E**) Quantitation of sliding assays ($n = 3$) shown in (A–D). Bands corresponding to remodeled nucleosomes were quantitated and normalized to their respective input bands (0 min) and plotted as mean ± s.e.m. (**F**) Model for the recruitment of Isw1b through the Ioc4 PWWP domain. In wildtype yeast the Ioc4 PWWP domain simultaneously interacts with H3K36 methylated nucleosomes and the nucleosomal DNA and thereby ensures recruitment of Ioc4 to gene bodies. The remodeler activity of Isw1b maintains proper nucleosome organization over ORFs which prevents the exposure of promoter-like elements (orange) and the appearance of cryptic transcripts. Without the Ioc4 PWWP domain (ΔPWWP) recruitment of Ioc4 to ORFs is severely curtailed and Isw1b cannot remodel nucleosomes effectively, which disrupts chromatin organization and results in inappropriate transcription initiation. Interfering with the ability of the PWWP domain to interact with DNA (2KE) has similar effects. The inability of an aromatic cage mutant (W22A) to recognize H3K36me3 or the absence of H3K36 methylation (*set2*) also interferes with Ioc4 recruitment. Interestingly, disruption of PWWP domain binding to methylated H3K36, DNA or both results in the same recruitment defects *in vivo*. The PWWP insertion motif promotes binding of the PWWP domain to DNA, histones and nucleosomes, yet its deletion does not lead to significant changes in Isw1b activity *in vitro* or *in vivo*.

Pdp1 and Pdp3 from fission yeast (12,28,29,32,42). Modeling of the Ioc4 PWWP domain onto the cryo-EM structure of LEDGF-PWWP (Figure 3) supports the notion that different subgroups of PWWP domains interact in similar fashion with nucleosomes by binding across the DNA gyres (32). It also visualizes convincingly that K149 and K150 are in close proximity to the nucleosomal DNA and that their mutation leads to a loss of binding of both DNA and nucleosomes.

Interestingly, the Ioc4 PWWP domain also binds to single-stranded RNA and hybrid RNA:DNA molecules with affinities comparable to that of double-stranded DNA (Figure 2). Whether nucleosomes and ssRNA or RNA:DNA molecules can be bound simultaneously remains unclear. However, it potentially further links Ioc4 and its PWWP domain to elongating RNAPII. In fact, the Isw1b subunits Ioc2 and Isw1 were shown to be able to interact with RNA specifically in RNA immunoprecipitation experiments, while Ioc4 was not investigated (31).

The second interesting feature of the Ioc4 PWWP domain is its remarkably long insertion motif which packs against the β-barrel. Some other PWWP domains also contain short insertions, yet their functions remain unclear. The insertion motif in the Ioc4 PWWP domain contributes both towards one of the basic patches involved in DNA binding as well as an acidic patch promoting PWWP domain binding to histones. Deletion of the insertion motif leads to the destabilization of the interactions between the PWWP domain with DNA, histones and nucleosomes (Figure 3). Our Ioc4 PWWP-nucleosome model places the insertion motif next to one of the nucleosomal DNA gyres as well as in close proximity to the histone H3 tail, in agreement with our *in vitro* experiments.

In addition to analyzing the PWWP domain on its own we have also evaluated its features in the context of full-length Ioc4 proteins as well as the entire Isw1b remodeler. Comparison with full-length Ioc4 shows that while the PWWP domain is responsible for the preferential binding to K36me3-containing nucleosomes, overall affinities are enhanced ca. 20-fold in the context of full-length Ioc4. Incorporation of Ioc4 into the Isw1b remodeler further increases the affinity of the remodeler for K36 trimethylated nucleosomes. This behavior agrees with the expectation that the Ioc subunits are responsible for guiding Isw1 remodelers towards target sites.

The integrity of the PWWP domain and its interactions with nucleosomal DNA as well as its association with methylated H3K36 all play important roles for Ioc4 localization *in vivo.* Disruption of PWWP domain binding to methylated H3K36 in a *set2*Δ mutant, as well as the aromatic cage mutant W22A, unable to recognize H3K36me3, show reduced localization *in vivo*. Similarly, the DNA-binding deficient 2KE mutant exhibits lower recruitment to ORFs. Combining the W22A and 2KE mutations had no further effect on *in vivo* localization beyond that shown by the single mutants (Figure 4).

Also, without the Ioc4 PWWP domain Isw1b remodels nucleosomes less effectively (Figure 6), disrupting chromatin organization and promoting the production of cryptic and antisense transcripts (Figure 5). Interfering with the ability of the PWWP domain to interact with DNA (2KE) or bind H3K36me3 (W22A) has similar effects, in agreement with the Ioc4 recruitment data (Figure 4).

Our previous work has shown that Isw1 and Isw1b in particular are required for the recycling of H3K36me3-modified histones over gene bodies during transcription, thus preventing the incorporation of soluble and highly acetylated histones which predispose yeast cells to the generation of non-coding transcripts. It has been suggested that Isw1b may stabilize existing nucleosomes after RNAPII passage, thereby retaining existing, H3K36 trimethylated histones (8). The mode of interaction between the Ioc4 PWWP domain and the nucleosome suggested by our model supports this interpretation. Indeed, in agreement with this idea we have some preliminary data to suggest that Ioc4 is able to stabilize nucleosomes *in vitro* under conditions that otherwise lead to their disintegration. Also, nucleosomal arrays in *isw1*Δ *chd1*Δ cells are known to be severely disrupted (43,44). More recently, a paper from the Clark Lab has shown that the Isw1b remodeler, together with Chd1 is important for resolving closely packed dinucleosomes (10). Failure to do so results in poor nucleosome phasing (10) which in turn could lead to the exposure of cryptic promoters that are usually inaccessible.

A number of PWWP domain-containing proteins have been identified in recent years. They are associated with a variety of protein (complexes) and involved in a diverse set of functions, such as DNA repair (29,45), transcriptional activation (46,47) and repression (3,27,48), DNA methyltransferases (12,49–51), histone lysine methyltransferases (52) and acetyltransferases (53–57) as well as limiting the spreading of heterochromatin (58,59). Many of these PWWP domains preferentially bind methylated histones, with particular emphasis on methylated H3K36 or H4K20 (3,15,48). A positively charged DNA-binding surface has been identified in several other PWWP domains and seems to represent a further common characteristic. The affinities for different PWWP domains and their substrates vary, although all of the domains studied bind nucleosomes with much higher affinities when compared to histone tail peptides. In general, the Ioc4 PWWP domain binds nucleosomes with lower affinity compared to domains from other proteins, such as LEDGF (23,24). However, most binding assays have focused on individual PWWP domains. We show that binding affinities for nucleosomes are greatly enhanced in the context of full-length Ioc4 and the entire Isw1b chromatin remodeler, while the PWWP domain promotes the recognition of K36 methylated nucleosomes and correct targeting for all constructs. Given that PWWP domains are fairly highly conserved, displaying most differences in the length of their insertion motifs and the N-terminal alpha-helical domain, the breadth of diverse molecular functions for these domains may seem somewhat surprising. However, the frequent co-occurrence of PWWP domains with other histone- or DNA-binding domains, such as PHD fingers, bromodomains, AT hooks or chromodomains can account for these differences (3,60) and underlines the importance of studying these domains in context whenever possible.

DATA AVAILABILITY

Gene Expression Omnibus: ChIP-chip data sets have been deposited with accession number GSE165984. Wildtype H3K36me3 ChIP-chip data were previously deposited with accession number GSE32044. Crystal coordinates were deposited with the Protein Data Bank (accession code 7E29).

SUPPLEMENTARY DATA

Supplementary Data are available at NAR Online.

ACKNOWLEDGEMENTS

We thank Julia Schluckebier for excellent technical assistance and Dr. Frits Kamp for help with CD experiments. Experiments were done using equipment in the BioPhysics Core Facility of the Biomedical Center, LMU. Crystallography data were collected at beamline BL17U at the SSRF, China.

Author contributions: J.L. purified and crystallized the Ioc4-PWWP domain. H.L. determined and analysed the structure. L.B. purified all other Ioc4 and Isw1b remodeler constructs and performed all *in vitro* experiments. K.W. and P.V. provided peptide-ligated histone octamers. A.R.A. performed RT-qPCR experiments. M.S. performed all other *in vivo* experiments. M.S. and M.G. performed bioinformatics analysis. M.S., H.L. and Y.L. supervised research. M.S. wrote the manuscript with input from all authors.

FUNDING

Science and Technology Planning Project of Shenzhen [JCYJ20180307155005435 to H.L.]; Deutsche Forschungsgmeinschaft [SFB1064, SM426/1-1 to M.S.]; Friedrich-Bauer-Stiftung [07/15]; Wellcome Trust [104175/Z/14/Z to P.V.]; European Research Council [ERC-STG grant 639253]; the Wellcome Centre for Cell Biology was supported by core funding from the Wellcome Trust [203149]; Edinburgh Protein Production Facility (EPPF) for their support; the EPPF was supported by the Wellcome Trust through a Multi-User Equipment grant [101527/Z/13/Z]. Funding for open access charge: Deutsche Forschungsgemeinschaft.

Conflict of interest statement. None declared.

REFERENCES

1. Hughes,A.L. and Rando,O.J. (2014) Mechanisms underlying nucleosome positioning in vivo. *Annu. Rev. Biophys.*, **43**, 41–63.
2. Smolle,M. and Workman,J.L. (2013) Transcription-associated histone modifications and cryptic transcription. *Biochim. Biophys. Acta*, **1829**, 84–97.
3. Qin,S. and Min,J. (2014) Structure and function of the nucleosome-binding PWWP domain. *Trends Biochem. Sci*, **39**, 536–547.
4. Narlikar,G.J., Sundaramoorthy,R. and Owen-Hughes,T. (2013) Mechanisms and functions of ATP-Dependent chromatin-remodeling enzymes. *Cell*, **154**, 490–503.
5. Elfring,L.K., Deuring,R., McCallum,C.M., Peterson,C.L. and Tamkun,J.W. (1994) Identification and characterization of drosophila relatives of the yeast transcriptional activator SNF2/SWI2. *Mol. Cell. Biol.*, **14**, 2225–2234.
6. Tsukiyama,T., Palmer,J., Landel,C.C., Shiloach,J. and Wu,C. (1999) Characterization of the imitation switch subfamily of ATP-dependent chromatin-remodeling factors in Saccharomyces cerevisiae. *Genes Dev.*, **13**, 686–697.
7. Vary,J.C. Jr, Gangaraju,V.K., Qin,J., Landel,C.C., Kooperberg,C., Bartholomew,B. and Tsukiyama,T. (2003) Yeast isw1p forms two separable complexes in vivo. *Mol. Cell. Biol.*, **23**, 80–91.
8. Smolle,M., Venkatesh,S., Gogol,M.M., Li,H., Zhang,Y., Florens,L., Washburn,M.P. and Workman,J.L. (2012) Chromatin remodelers isw1 and Chd1 maintain chromatin structure during transcription by preventing histone exchange. *Nat. Struct. Mol. Biol.*, **19**, 884–892.
9. Venkatesh,S., Smolle,M., Li,H., Gogol,M., Saint,M., Kumar,S., Natarajan,K. and Workman,J.L. (2012) Set2 methylation of histone H3 lysine36 suppresses histone exchange on transcribed genes. *Nature*, **489**, 452–455.
10. Eriksson,P.R. and Clark,D.J. (2021) The yeast ISW1b ATP-dependent chromatin remodeler is critical for nucleosome spacing and dinucleosome resolution. *Sci. Rep.*, **11**, 4195.
11. Maurer-Stroh,S., Dickens,N.J., Hughes-Davies,L., Kouzarides,T., Eisenhaber,F. and Ponting,C.P. (2003) The tudor domain 'Royal family': tudor, plant agenet, chromo, PWWP and MBT domains. *Trends Biochem. Sci*, **28**, 69–74.
12. Qiu,C., Sawada,K., Zhang,X. and Cheng,X. (2002) The PWWP domain of mammalian DNA methyltransferase Dnmt3b defines a new family of DNA-binding folds. *Nat. Struct. Biol.*, **9**, 217–224.
13. Ge,Y.Z., Pu,M.T., Gowher,H., Wu,H.P., Ding,J.P., Jeltsch,A. and Xu,G.L. (2004) Chromatin targeting of de novo DNA methyltransferases by the PWWP domain. *J. Biol. Chem.*, **279**, 25447–25454.
14. Wu,H., Zeng,H., Lam,R., Tempel,W., Amaya,M.F., Xu,C., Dombrovski,L., Qiu,W., Wang,Y. and Min,J. (2011) Structural and histone binding ability characterizations of human PWWP domains. *PLoS One*, **6**, e18919.
15. Wang,Y., Reddy,B., Thompson,J., Wang,H., Noma,K., Yates,J.R. 3rd and Jia,S. (2009) Regulation of Set9-mediated H4K20 methylation by a PWWP domain protein. *Mol. Cell*, **33**, 428–437.
16. Li,B., Gogol,M., Carey,M., Lee,D., Seidel,C. and Workman,J.L. (2007) Combined action of PHD and chromo domains directs the Rpd3S HDAC to transcribed chromatin. *Science (New York, N.Y.)*, **316**, 1050–1054.
17. Voigt,P., LeRoy,G., Drury,W.J. 3rd, Zee,B.M., Son,J., Beck,D.B., Young,N.L., Garcia,B.A. and Reinberg,D. (2012) Asymmetrically modified nucleosomes. *Cell*, **151**, 181–193.
18. Thastrom,A., Bingham,L.M. and Widom,J. (2004) Nucleosomal locations of dominant DNA sequence motifs for histone-DNA interactions and nucleosome positioning. *J. Mol. Biol.*, **338**, 695–709.
19. Li,B., Gogol,M., Carey,M., Pattenden,S.G., Seidel,C. and Workman,J.L. (2007) Infrequently transcribed long genes depend on the Set2/Rpd3S pathway for accurate transcription. *Genes Dev.*, **21**, 1422–1430.
20. Carrozza,M.J., Li,B., Florens,L., Suganuma,T., Swanson,S.K., Lee,K.K., Shia,W.J., Anderson,S., Yates,J., Washburn,M.P. *et al.* (2005) Histone H3 methylation by Set2 directs deacetylation of coding regions by Rpd3S to suppress spurious intragenic transcription. *Cell*, **123**, 581–592.
21. Maltby,V.E., Martin,B.J., Schulze,J.M., Johnson,I., Hentrich,T., Sharma,A., Kobor,M.S. and Howe,L. (2012) Histone H3 lysine 36 methylation targets the Isw1b remodeling complex to chromatin. *Mol. Cell. Biol.*, **32**, 3479–3485.
22. Pinskaya,M., Nair,A., Clynes,D., Morillon,A. and Mellor,J. (2009) Nucleosome remodeling and transcriptional repression are distinct functions of Isw1 in Saccharomyces cerevisiae. *Mol. Cell. Biol.*, **29**, 2419–2430.
23. van Nuland,R., van Schaik,F.M., Simonis,M., van Heesch,S., Cuppen,E., Boelens,R., Timmers,H.M. and van Ingen,H. (2013) Nucleosomal DNA binding drives the recognition of H3K36-methylated nucleosomes by the PSIP1-PWWP domain. *Epigenetics Chromatin*, **6**, 12.
24. Eidahl,J.O., Crowe,B.L., North,J.A., McKee,C.J., Shkriabai,N., Feng,L., Plumb,M., Graham,R.L., Gorelick,R.J., Hess,S. *et al.* (2013) Structural basis for high-affinity binding of LEDGF PWWP to mononucleosomes. *Nucleic Acids Res.*, **41**, 3924.
25. Tian,W., Yan,P., Xu,N., Chakravorty,A., Liefke,R., Xi,Q. and Wang,Z. (2019) The HRP3 PWWP domain recognizes the minor

groove of double-stranded DNA and recruits HRP3 to chromatin. *Nucleic Acids Res.*, **47**, 5436–5448.
26. Rona,G.B., Eleutherio,E.C.A. and Pinheiro,A.S. (2016) PWWP domains and their modes of sensing DNA and histone methylated lysines. *Biophys. Rev.*, **8**, 63–74.
27. Yang,J. and Everett,A.D. (2007) Hepatoma-derived growth factor binds DNA through the N-terminal PWWP domain. *BMC Mol. Biol.*, **8**, 101.
28. Qiu,Y., Zhang,W., Zhao,C., Wang,Y., Wang,W., Zhang,J., Zhang,Z., Li,G., Shi,Y., Tu,X. *et al.* (2012) Solution structure of the Pdp1 PWWP domain reveals its unique binding sites for methylated H4K20 and DNA. *Biochem. J.*, **442**, 527–538.
29. Laguri,C., Duband-Goulet,I., Friedrich,N., Axt,M., Belin,P., Callebaut,I., Gilquin,B., Zinn-Justin,S. and Couprie,J. (2008) Human mismatch repair protein MSH6 contains a PWWP domain that targets double stranded DNA. *Biochemistry*, **47**, 6199–6207.
30. Lukasik,S.M., Cierpicki,T., Borloz,M., Grembecka,J., Everett,A. and Bushweller,J.H. (2006) High resolution structure of the HDGF PWWP domain: a potential DNA binding domain. *Protein Sci.*, **15**, 314–323.
31. Babour,A., Shen,Q., Dos-Santos,J., Murray,S., Gay,A., Challal,D., Fasken,M., Palancade,B., Corbett,A., Libri,D. *et al.* (2016) The chromatin remodeler ISW1 is a quality control factor that surveys nuclear mRNP biogenesis. *Cell*, **167**, 1201–1214.
32. Wang,H., Farnung,L., Dienemann,C. and Cramer,P. (2020) Structure of H3K36-methylated nucleosome-PWWP complex reveals multivalent cross-gyre binding. *Nat. Struct. Mol. Biol.*, **27**, 8–13.
33. Chabbert,C.D., Adjalley,S.H., Klaus,B., Fritsch,E.S., Gupta,I., Pelechano,V. and Steinmetz,L.M. (2015) A high-throughput ChIP-Seq for large-scale chromatin studies. *Mol. Syst. Biol.*, **11**, 777.
34. Sayou,C., Millán-Zambrano,G., Santos-Rosa,H., Petfalski,E., Robson,S., Houseley,J., Kouzarides,T. and Tollervey,D. (2017) RNA binding by histone methyltransferases Set1 and Set2. *Mol. Cell. Biol.*, **37**, e00165-17.
35. Cole,H.A., Ocampo,J., Iben,J.R., Chereji,R.V. and Clark,D.J. (2014) Heavy transcription of yeast genes correlates with differential loss of histone H2B relative to H4 and queued RNA polymerases. *Nucleic Acids Res.*, **42**, 12512–12522.
36. Weiner,A., Hughes,A., Yassour,M., Rando,O.J. and Friedman,N. (2010) High-resolution nucleosome mapping reveals transcription-dependent promoter packaging. *Genome Res.*, **20**, 90–100.
37. Kireeva,M.L., Walter,W., Tchernajenko,V., Bondarenko,V., Kashlev,M. and Studitsky,V.M. (2002) Nucleosome remodeling induced by RNA polymerase II: loss of the H2A/H2B dimer during transcription. *Mol. Cell*, **9**, 541–552.
38. Belotserkovskaya,R., Oh,S., Bondarenko,V.A., Orphanides,G., Studitsky,V.M. and Reinberg,D. (2003) FACT facilitates transcription-dependent nucleosome alteration. *Science*, **301**, 1090–1093.
39. Guan,M., Xia,P., Tian,M., Chen,D. and Zhang,X. (2020) Molecular fingerprints of conazoles via functional genomic profiling of Saccharomyces cerevisiae. *Toxicol. In Vitro*, **69**, 104998.
40. Quan,T.K. and Hartzog,G.A. (2010) Histone H3K4 and K36 methylation, Chd1 and Rpd3S oppose the functions of Saccharomyces cerevisiae Spt4-Spt5 in transcription. *Genetics*, **184**, 321–334.
41. Stockdale,C., Flaus,A., Ferreira,H. and Owen-Hughes,T. (2006) Analysis of nucleosome repositioning by yeast ISWI and Chd1 chromatin remodeling complexes. *J. Biol. Chem.*, **281**, 16279–16288.
42. Georgescu,P.R., Capella,M., Fischer-Burkart,S. and Braun,S. (2020) The euchromatic histone mark H3K36me3 preserves heterochromatin through sequestration of an acetyltransferase complex in fission yeast. *Microb Cell*, **7**, 80–92.
43. Gkikopoulos,T., Schofield,P., Singh,V., Pinskaya,M., Mellor,J., Smolle,M., Workman,J.L., Barton,G.J. and Owen-Hughes,T. (2011) A role for Snf2-related nucleosome-spacing enzymes in genome-wide nucleosome organization. *Science (New York, N.Y.)*, **333**, 1758–1760.
44. Ocampo,J., Chereji,R.V., Eriksson,P.R. and Clark,D.J. (2016) The ISW1 and CHD1 ATP-dependent chromatin remodelers compete to set nucleosome spacing in vivo. *Nucleic Acids Res.*, **44**, 4625–4635.
45. Huang,Y., Gu,L. and Li,G.M. (2018) H3K36me3-mediated mismatch repair preferentially protects actively transcribed genes from mutation. *J. Biol. Chem.*, **293**, 7811–7823.
46. Zhu,X., Lan,B., Yi,X., He,C., Dang,L., Zhou,X., Lu,Y., Sun,Y., Liu,Z., Bai,X. *et al.* (2020) HRP2-DPF3a-BAF complex coordinates histone modification and chromatin remodeling to regulate myogenic gene transcription. *Nucleic Acids Res.*, **48**, 6563–6582.
47. Fei,J., Ishii,H., Hoeksema,M.A., Meitinger,F., Kassavetis,G.A., Glass,C.K., Ren,B. and Kadonaga,J.T. (2018) NDF, a nucleosome-destabilizing factor that facilitates transcription through nucleosomes. *Genes Dev.*, **32**, 682–694.
48. Wen,H., Li,Y., Xi,Y., Jiang,S., Stratton,S., Peng,D., Tanaka,K., Ren,Y., Xia,Z., Wu,J. *et al.* (2014) ZMYND11 links histone H3.3K36me3 to transcription elongation and tumour suppression. *Nature*, **508**, 263–268.
49. Chen,T., Tsujimoto,N. and Li,E. (2004) The PWWP domain of Dnmt3a and Dnmt3b is required for directing DNA methylation to the major satellite repeats at pericentric heterochromatin. *Mol. Cell. Biol.*, **24**, 9048–9058.
50. Otani,J., Nankumo,T., Arita,K., Inamoto,S., Ariyoshi,M. and Shirakawa,M. (2009) Structural basis for recognition of H3K4 methylation status by the DNA methyltransferase 3A ATRX-DNMT3-DNMT3L domain. *EMBO Rep.*, **10**, 1235–1241.
51. Weinberg,D.N., Papillon-Cavanagh,S., Chen,H., Yue,Y., Chen,X., Rajagopalan,K.N., Horth,C., McGuire,J.T., Xu,X., Nikbakht,H. *et al.* (2019) The histone mark H3K36me2 recruits DNMT3A and shapes the intergenic DNA methylation landscape. *Nature*, **573**, 281–286.
52. He,C., Li,F., Zhang,J., Wu,J. and Shi,Y. (2013) The methyltransferase NSD3 has chromatin-binding motifs, PHD5-C5HCH, that are distinct from other NSD (nuclear receptor SET domain) family members in their histone H3 recognition. *J. Biol. Chem.*, **288**, 4692–4703.
53. Vezzoli,A., Bonadies,N., Allen,M.D., Freund,S.M., Santiveri,C.M., Kvinlaug,B.T., Huntly,B.J., Gottgens,B. and Bycroft,M. (2010) Molecular basis of histone H3K36me3 recognition by the PWWP domain of Brpf1. *Nat. Struct. Mol. Biol.*, **17**, 617–619.
54. Laue,K., Daujat,S., Crump,J.G., Plaster,N., Roehl,H.H., Tubingen Screen,C., Kimmel,C.B., Schneider,R. and Hammerschmidt,M. (2008) The multidomain protein Brpf1 binds histones and is required for Hox gene expression and segmental identity. *Development*, **135**, 1935–1946.
55. Liu,L., Qin,S., Zhang,J., Ji,P., Shi,Y. and Wu,J. (2012) Solution structure of an atypical PHD finger in BRPF2 and its interaction with DNA. *J. Struct. Biol.*, **180**, 165–173.
56. Poplawski,A., Hu,K., Lee,W., Natesan,S., Peng,D., Carlson,S., Shi,X., Balaz,S., Markley,J.L. and Glass,K.C. (2014) Molecular insights into the recognition of N-terminal histone modifications by the BRPF1 bromodomain. *J. Mol. Biol.*, **426**, 1661–1676.
57. Qin,S., Jin,L., Zhang,J., Liu,L., Ji,P., Wu,M., Wu,J. and Shi,Y. (2011) Recognition of unmodified histone H3 by the first PHD finger of bromodomain-PHD finger protein 2 provides insights into the regulation of histone acetyltransferases monocytic leukemic zinc-finger protein (MOZ) and MOZ-related factor (MORF). *J. Biol. Chem.*, **286**, 36944–36955.
58. Dou,K., Liu,Y., Zhang,Y., Wang,C., Huang,Y. and Zhang,Z.Z. (2020) Drosophila P75 safeguards oogenesis by preventing H3K9me2 spreading. *J. Genet. Genomics*, **47**, 187–199.
59. Albig,C., Wang,C., Dann,G.P., Wojcik,F., Schauer,T., Krause,S., Maenner,S., Cai,W., Li,Y., Girton,J. *et al.* (2019) JASPer controls interphase histone H3S10 phosphorylation by chromosomal kinase JIL-1 in drosophila. *Nat. Commun.*, **10**, 5343.
60. Savitsky,P., Krojer,T., Fujisawa,T., Lambert,J.P., Picaud,S., Wang,C.Y., Shanle,E.K., Krajewski,K., Friedrichsen,H., Kanapin,A. *et al.* (2016) Multivalent histone and DNA engagement by a PHD/BRD/PWWP triple reader cassette recruits ZMYND8 to K14ac-rich chromatin. *Cell Rep.*, **17**, 2724–2737.